Proceedings of ASME FEDSM'02
ASME 2002 Fluids Engineering Division Summer Meeting
Montreal, Quebec, Canada, July 14-18, 2002

FEDSM2002-31024

SIMILITUDE OF AIR ENTRAINMENT AT VERTICAL CIRCULAR PLUNGING JETS

Hubert CHANSON
Dept. of Civil Eng., The University of Queensland, Brisbane QLD 4072, Australia

Shin-ichi AOKI
Dept. of Architecture and Civil Eng., Toyohashi University of Technology, Toyohashi 441-8580, Japan

Ashabul HOQUE
Dept. of Architecture and Civil Eng., Toyohashi University of Technology, Toyohashi 441-8580, Japan

ABSTRACT

Air bubble entrainment at plunging jet takes place when the jet impact velocity exceeds a critical velocity function of the inflow conditions. This study investigates scale effects affecting air entrainment and bubble dispersion at vertical circular plunging jets. Three scale models were used and detailed air-water measurements were performed systematically for identical Froude numbers. The results highlight significant scale effects when $We_1 < 1E+3$ or $V_1/u_r < 10$. Bubble chord times were also measured and presented in terms of pseudo-bubble chord length which was found to overestimate real bubble chords by 10 to 30%. The data show pseudo-bubble chord sizes ranging from less than 0.5 mm to more than 10 mm. The average pseudo-chord sizes were between 5 and 7 mm.

Keywords : Air bubble entrainment, plunging jet, physical modelling, scale effects.

INTRODUCTION

At the intersection of a plunging jet with a pool of water, free-surface instabilities develop and air bubble entrainment may be observed (Fig. 1). This is a form of local, singular aeration (CHANSON 1997). Plunging jet flow situations are encountered in Nature (e.g. at impact of waterfalls). Industrial applications of plunging jets include minerals-processing flotation cells, waste-water treatment, oxygenation of mammalian-cell bio-reactors and riverine re-oxygenation weirs (e.g. CHANSON 1997, KOLANI et al. 1998). In the oceans, plunging breaking waves can entrain a large amount of air bubbles when the top of the wave forms a water jet projecting ahead and impacts the water free-surface in front of the wave (e.g. GRIFFIN 1984).

Several studies showed that air entrainment at plunging jets takes place when the jet impact velocity exceeds a characteristic velocity V_e which is a function of the inflow conditions (e.g. ERVINE et al. 1980, CUMMINGS and CHANSON 1999). The mechanisms of bubble entrainment depends upon the jet velocity at impact, the fluid properties, the nozzle design, the free-falling jet length and the jet turbulence. For small jet velocities larger than the onset velocity, air is entrained in the form of individual air bubbles. At larger jet velocities, large packets of air are entrained and broken up subsequently in the shear flow (e.g. BIN 1993, CUMMINGS and CHANSON 1997a, CHANSON and BRATTBERG 1998, ZHU et al. 2000). At the impingement perimeter, the bubble entrapment is highly unsteady, affecting the stability of the complete system : i.e., jet and receiving pool.

Dimensional analysis

Laboratory studies of air-water flows require the selection of an adequate similitude. Considering air bubble entrainment at vertical plunging water jets, the relevant parameters needed for any dimensional analysis include fluid properties and physical constants, channel (or flow) geometry, upstream flow properties, air-water flow properties. It yields :

$$F\left(C ; Fr ; Tu ; \frac{d_{ab}}{d_1} ; \frac{x_1}{d_1} ; Fr_1 ; We_1 ; Tu_1 ; Mo\right) = 0 \qquad (1)$$

where C is the void fraction, $Fr = V/\sqrt{g * d_1}$, V is the velocity, d_1 is the jet impact diameter, x_1 is the free-jet length, Tu is the turbulence intensity, d_{ab}/d_1 is a dimensionless characteristic bubble size. The dimensionless inflow variables are $Fr_1 = V_1/\sqrt{g * d_1}$, $We_1 = \rho_w * V_1^2 * d_1/\sigma$ and Tu_1 while $Mo = (g*\mu_w^4)/(\rho_w*\sigma^3)$ is the Morton number also called liquid parameter. In Equation (1), C, Fr, Tu and d_{ab}/d_1 are dimensionless characteristics

of the flow field below impingement.

Fig. 1 - Photograph of air bubble entrainment at plunging jet (V_1 = 2.2 m/s, x_1 = 0.5 m, Model 2)

Fig. 2 - Sketch of air entrainment at vertical circular plunging jet

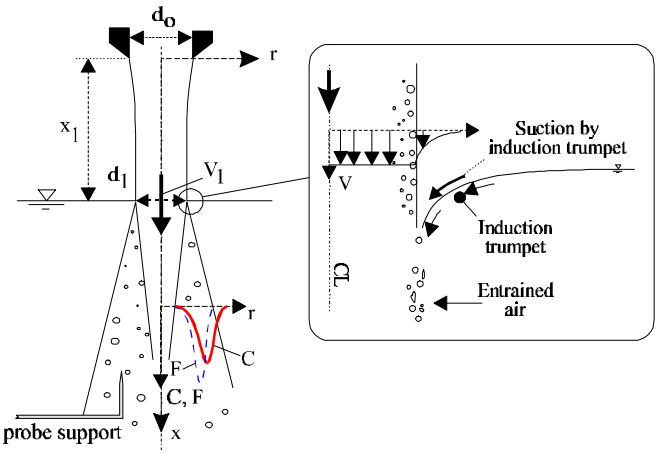

In free-surface flows, gravity effects are important and most laboratory studies are based upon a Froude similitude (HENDERSON 1966, CHANSON 1999). The entrapment of air bubbles and the mechanisms of bubble breakup and coalescence are dominated by surface tension effects implying the need for Weber similitude (WOOD 1991, CHANSON 1997). For geometrically-similar models, it is impossible to satisfy simultaneously Froude and Weber similarities with the same fluids in model and prototype. In small size models based upon a Froude similitude, the air entrainment process may be underestimated. WOOD (1991) and CHANSON (1997) discussed such scale effects. KOBUS (1984) presented some applications.

This study reviews basic air entrainment characteristics at vertical circular plunging jets. Three scale models were built and detailed experiments were performed for a wide range of flow situations. The results presents new evidence leading to a better understanding of scale effects affecting the air entrainment process.

NOMENCLATURE

C air concentration, also called void fraction;
C_{max} maximum void fraction in a cross-section;
ch_{ab} pseudo-bubble chord length (m);
D_t turbulent diffusivity (m^2/s) of air bubbles;
$D^{\#}$ dimensionless turbulent diffusivity : $D^{\#} = D_t/(V_1*r_1)$;
d circular jet diameter;
d_{ab} air bubble diameter (m);
d_o nozzle diameter (m);
F bubble count rate or bubble frequency (Hz);
Fr Froude number defined as : $Fr = V/\sqrt{g * d}$;
g gravity constant (m/s^2);
Mo Morton number defined as : $Mo = (g*\mu_w^4)/(\rho_w*\sigma^3)$;
Q_w water discharge (m^3/s);
Q_{air} quantity of entrained air (m^3/s);
r radial distance (m) from the centreline;
r_1 jet radius (m) at impingement point : $r_1 = d_1/2$;
Tu turbulence intensity defined as : Tu = u'/V;
t_{ch} bubble chord time (s);
u_r bubble rise velocity (m/s);
u' std of longitudinal turbulent velocity (m/s);
V velocity (m/s);
V_e onset velocity (m/s) for air entrainment;
W channel width (m);
We Weber number : $We = \rho_w * V^2 * d/\sigma$;
x distance along the flow direction (m);
x_1 distance (m) between nozzle and impingement point;
Y_{Cmax} radial distance (m) where $C = C_{max}$;
μ_w dynamic viscosity (Pa.s);
ρ_w density (kg/m^3);
σ surface tension between air and water (N/m);

Subscript
1 inflow conditions (i.e. at impingement).

EXPERIMENTAL FACILITIES

Two experimental facilities were used to provide three circular plunging jet configurations called Models 1, 2 and 3 (Table 1, Fig. 1). Experiments were conducted with tap water and ambient air. In Model 1, the receiving channel was 0.3 m wide, 3.6 m long and 1.8 m deep with glass walls. The circular nozzle was made of aluminium with a 1/2.16 contraction ratio. In Models 2 and 3, the receiving flume was 0.10 m wide, 0.75 m deep and 2 m long. The nozzle was sharp-edged, being machined with an accuracy less than 0.1 mm and the water was supplied by a straight circular vertical PVC pipe.

In Model 1, the discharge was measured with an orifice meter (British Standards design) calibrated on-site with a volume-per-time technique. The flow rate was measured

with a volume per time technique in Models 2 and 3. The error on the discharge measurement was less than 2%. In the largest facility (Model 1), clear water jet velocities and turbulent velocity fluctuations were measured in the free-falling jet using a Prandtl-Pitot tube (diameter 3.3 mm) and a conical hot-film probe system (Dantec 55R42, 0.3 mm size).

Air-water flow properties were measured with single-tip conductivity probes (needle probe design). In Model 1, the probe (inner electrode: ∅ = 0.35 mm) signal was scanned at 5 kHz for three minutes. In Models 2 and 3, a Kanomax™ System 7931 resistivity probe was used (inner electrode ∅ = 0.1 mm). Void fraction and bubble count rates were calculated by analog integration for five minutes. In Model 2, raw probe outputs were also recorded at 25 kHz to calculate bubble chord time distributions.

Table 1- Summary of experimental flow conditions

d_o m (1)	x_1 m (2)	Inception condition (3)	V_1 m/s (4)	Fr_1 (5)	Tu_1 (6)	Comments (7)
Model 1						
0.025	0.1	V_e = 1.58 m/s, Tu_1 = 0.47%	3.5 4.1 4.4	7.2 8.4 9.0	0.39% 0.46% 0.96%	Tap water (σ = 0.055 N/m). Inflow pipe: 3.5 m long. Water depth: ~1.5 m.
Model 2						
0.0125	0.05	V_e = 1.03 m/s	2.42 3.04 3.18 3.46	7.1 8.8 9.2 10.0	N/A	Tap water (σ = 0.073 N/m). Inflow pipe : 1.2 m long. Water depth: ~0.65 m.
Model 3						
0.0068	0.027	V_e = 0.73 m/s	1.79 2.16 2.30 2.49	7.1 8.5 9.0 9.7	N/A	Tap water (σ = 0.073 N/m). Inflow pipe : 1 m long. Water depth: ~0.65 m.

Notes : Tu_1 : turbulence intensity of the jet core at impact; σ : measured surface tension between air and water.

Measurements were taken on the jet diameter through the centreline. In each Model at each cross-section, the probe sensor and support were initially located at $r < -d_1$ and measurements were conducted by moving the probe tip with increasing radial coordinate r (Fig. 2). The displacement of the probes in the flow direction and direction normal to the jet support was controlled by fine adjustment travelling mechanisms. The error in the probe position was less than 0.2 mm in each direction. Further details on the experiments were reported in CHANSON et al. (2002).

Design procedure

The models were designed to be geometrically similar based upon a Froude similitude with undistorted scale. The geometric scaling ratio between Model 1 and Model 2 was 2.0, and the scaling ratio was 3.66 between Models 1 and 3. Similar experiments were conducted for identical inflow Froude numbers Fr_1. Measurements were performed at similar cross-sections $(x-x_1)/r_1$ where x is the longitudinal coordinate and r_1 is the jet impact radius ($r_1 = d_1/2$, Fig. 2).

BASIC FLOW PATTERNS

Each model exhibited similar flow patterns. For all the experiments, the free jet was transparent up to impingement. No entrained bubbles could be seen but some small longitudinal streaks were visible at the free-surface. For very low velocity V_1, no air was entrained at jet impact. With increasing jet velocities, all the other parameters being unchanged, individual bubble entrainment was seen. The inception conditions for air bubble entrainment were measured and reported in Table 1, column 3. The results for Models 1 and 2 were consistent with previous results (ERVINE et al. 1980, CUMMINGS and CHANSON 1999). In Model 3, the flow conditions at inception were visually different. The free jet surface was smooth, followed by free-surface annular waves developing in the flow direction similar to wavy flow patterns illustrated by BRENNEN (1970) and HOYT and TAYLOR (1977). It is believed that the inflow was laminar.

For a jet velocity slightly greater than the inception velocity, individual air bubble entrainment was observed. Most entrapped bubbles were visually small (i.e. with diameter less than 0.5 to 1 mm) and tended to follow a slightly helicoidal trajectory around the jet centreline. For larger jet velocities ($V_1 > V_e$), an unstable air cavity developed at one point along the impingement perimeter. The air cavity position changed with time in an apparently random manner. Large air packets were entrained below the air cavity with the stretching and breakup of the cavity tip. Visual observations showed predominantly entrained bubble sizes between 0.5 and 5 mm. Such millimetric size bubbles have a nearly constant bubble rise velocity : i.e., $u_r \approx 0.25$ to 0. 3 m/s (COMOLET 1979). At larger speeds, the air cavity developed all around the perimeter and most air was entrained by elongation, stretching and breakup of the ventilated cavity (Fig. 2). Visually most entrained bubbles tended to follow a somewhat helicoidal trajectory.

Although the bulk of entrained bubbles did not penetrate deeply and never reached the bottom of the flume, fine bubbles with sizes less than 0.5 to 1 mm were consistently observed at deeper depths. Visual observations showed tiny bubbles trapped in large vortical structures for a relatively long time before being ejected to another eddy or toward the free-surface.

DISTRIBUTIONS OF VOID FRACTIONS AND BUBBLE COUNT RATES

In the developing flow region, the distributions of void fraction exhibited smooth, derivative profiles (Fig. 3 & 4). Figure 3 presents data for an impact Froude number $Fr_1 = 9$ and Figure 4 shows data for smaller jet velocities (i.e. $Fr_1 = 7$). The data illustrate the advective diffusion of entrained air associated with an quasi-exponential decay of the maximum air content with longitudinal distance from impingement and

a broadening of the air diffusion layer. For all experiments, the data may be fitted by a simple analytical solution of the advective diffusion equation for air bubbles :

Fig. 3 - Dimensionless distributions of void fractions C and bubble count rates F^*r_1/V_1 for Fr_1 = 9 - Comparison between Model 1 (run BM44_2), Model 2 (run CIR5_5), Model 3 (Run-2) and Equation (2) : (Top) $(x-x_1)/r_1$ = 1.6, (Middle) $(x-x_1)/r_1$ = 2.4, (Bottom) $(x-x_1)/r_1$ = 4.0

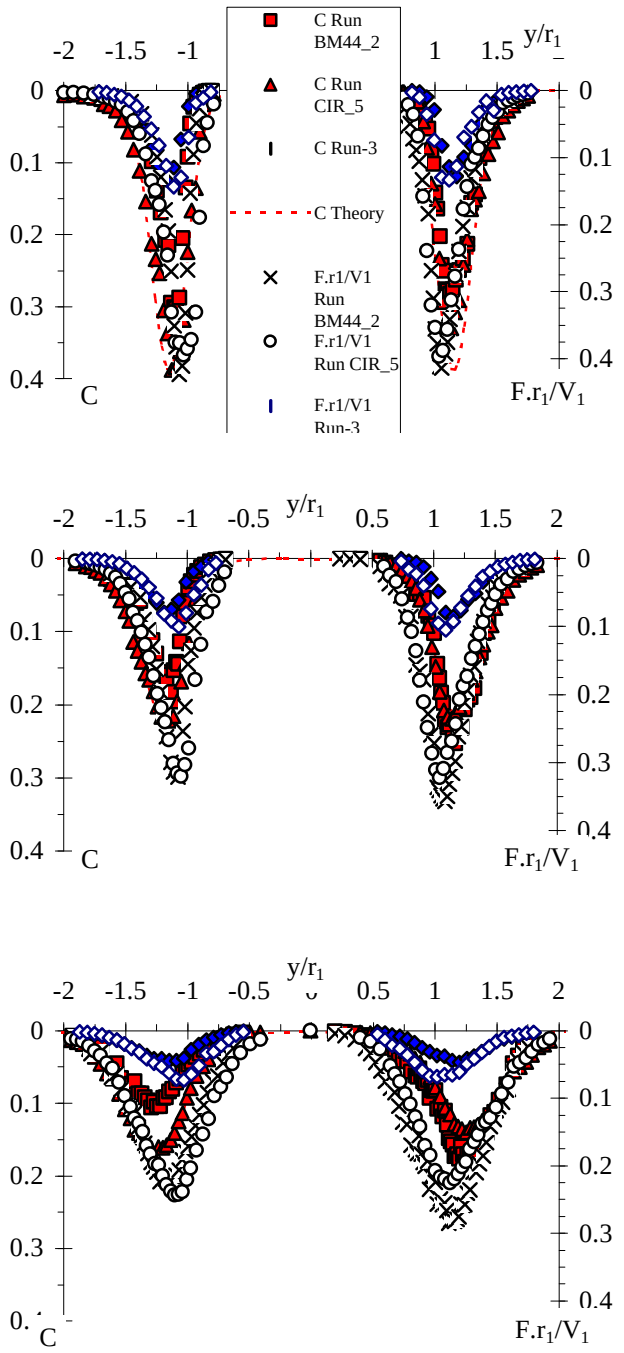

$$C = \frac{Q_{air}}{Q_w} * \frac{1}{4 * D^{\#} * \frac{x - x_1}{Y_{Cmax}}} * \exp\left(- \frac{1}{4 * D^{\#}} * \frac{\left(\frac{r}{Y_{Cmax}}\right)^2 + 1}{\frac{x - x_1}{Y_{Cmax}}} \right) * I_o\left(\frac{1}{2 * D^{\#}} * \frac{\frac{r}{Y_{Cmax}}}{\frac{x - x_1}{Y_{Cmax}}} \right) \quad (2)$$

where Q_w is the water flow rate, Q_{air} is the air flux, x is the longitudinal coordinate and r is the radial distance (Fig. 2), $D^{\#}$ is a dimensionless air bubble diffusivity, $Y_{Cmax} = r(C=C_{max})$ and I_o is the modified Bessel function of the first kind of order zero (CHANSON 1997). Equation (2) is compared with Models 1 and 2 data on Figures 3 & 4. Values of $D^{\#}$ and Q_{air}/Q_w were determined from best fit.

Fig. 4 - Dimensionless distributions of void fractions C and bubble count rates F^*r_1/V_1 for Fr_1 = 7 - Comparison between Model 1 (run BM35_1), Model 2 (run CIR2_5), Model 3 (Run-3) and Equation (2) : (Top) $(x-x_1)/r_1$ = 1.6, (Bottom) $(x-x_1)/r_1$ = 2.4, (c) $(x-x_1)/r_1$ = 4.0

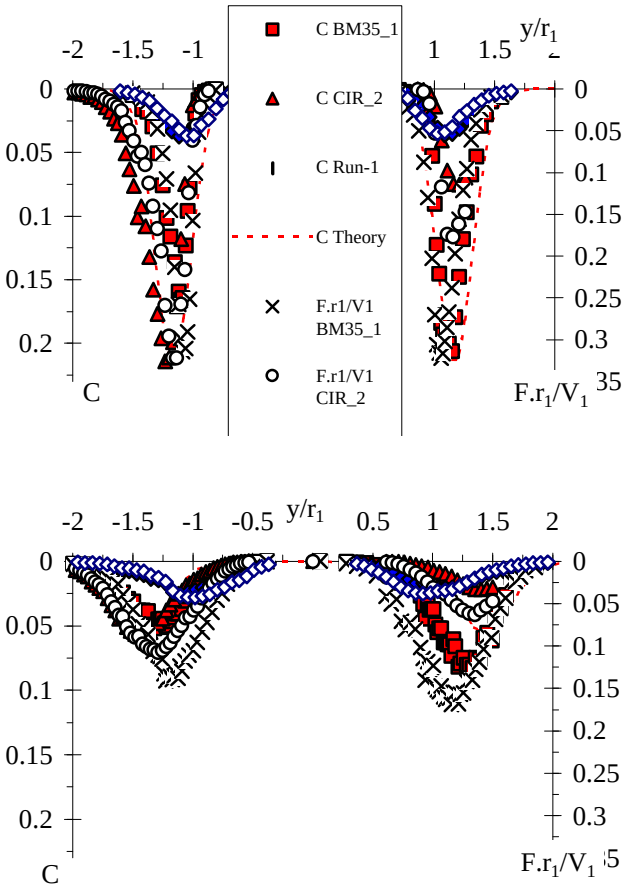

Distributions of bubble count rates are also shown (Fig. 3 & 4). For all experiments, the results highlighted maximum bubble frequency in the developing shear layers. The

maximum bubble count rate occurred consistently in the inner shear region: i.e., at a distance from the jet centreline that was smaller than the location Y_{Cmax} where the void fraction was maximum. Such a result was previously observed with two-dimensional jets (BRATTBERG and CHANSON 1998). BRATTBERG and CHANSON assumed that this was caused by "*the non-coincidence between the air bubble diffusion layer and the momentum shear layer*".

Fig. 5 - Pseudo-bubble chord length distributions ($ch_{ab} = V_1 * t_{ch}$) - Model 2, $Fr_1 = 9.1$, $x_1/d_o = 4$

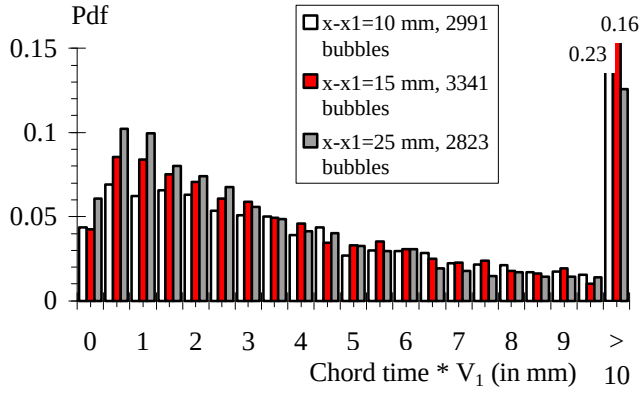

BUBBLE CHORD TIME DISTRIBUTIONS

The bubble chord time is defined as the time spent by a bubble on the probe sensor. Chord time data were calculated from the raw signal scanned at 25 kHz for 2.6 seconds at 8 locations per cross-section. The results are presented in terms of pseudo-bubble chord length ch_{ab} defined as :

$$ch_{ab} = V_1 * t_{ch} \quad (3)$$

where t_{ch} is the bubble chord time. CHANSON et al. (2002) showed that Equation (3) overestimates the bubble chord lengths by about 10 to 30%. Pseudo-bubble chord length data are shown in Figure 5 for one experiment at three cross-sections: $(x-x_1)/r_1 = 1.6$, 2.4 & 4.0. At each cross-section, the histograms describe all bubbles detected across the shear layer width (i.e. 8 locations). In Figure 5, each histogram column represents the probability of chord length in 0.5 mm intervals : e.g., the probability of a chord length from 2.0 to 2.5 mm is represented by the column labelled 2.0. The last column (i.e. > 10) indicates the probability of chord lengths exceeding 10 mm.

The data demonstrate the broad spectrum of pseudo-bubble chord lengths at each cross-section : i.e., from less than 0.5 mm to larger than 10 mm (Fig. 5). The pseudo-bubble chord length distributions are skewed with a preponderance of small bubble sizes relative to the mean. The probability of bubble chord length is the largest for bubble sizes between 0 and 2 mm although the mean pseudo-chord size is typically 5 to 7 mm for all Models. It is worth noting the large fraction of bubbles larger than 10 mm next to the impingement perimeter : i.e., at $x-x_1 = 10$ mm (Fig. 5). These large bubbles may be large air packets entrapped at impingement which are subsequently broken up by turbulent shear.

The results show further that, at a given cross-section, the mean chord size increases with increasing jet velocity. The trend characterises the entrainment of larger air packets with increasing impact velocity V_1 and it is consistent with two-dimensional plunging jet observations (e.g. CUMMINGS and CHANSON 1997b).

DISCUSSION. SCALE EFFECTS

Experiments were conducted with three geometric scales based upon a Froude similitude with undistorted geometric scale. For identical fluids in all three Models, the Froude similitude implies that the Weber number differs between experiments and that surface tension-dominated processes may not be properly scaled. In the present study, identical results were basically observed between Models 1 and 2 at each cross-section for $Fr_1 = 8.5$ and 9. Some differences were noted for the lowest Froude number ($Fr_1 = 7$) (Fig. 4). That is, a faster decay of void fraction and bubble count rate with distance $(x-x_1)/r_1$ in Model 2. The trend suggests a greater detrainment rate in Model 2 because the bubble rise velocity cannot be scaled properly with a Froude similitude, and the rise velocity was nearly identical in all Models. Based upon the present study, it is suggested that scale effects in terms of detrainment occur for $V_1/u_r < 10$, where u_r is the characteristic rise velocity of entrained air bubbles.

Model 3 data showed consistently lesser entrained air than the two larger models. That is, lesser void fractions and dimensionless bubble count rates for identical inflow conditions. The observations imply that the rate of air entrainment was underestimated in Model 3 and hence the experiments were affected by scale effects. For the range of investigated flow conditions (Table 1), air entrainment at vertical circular jets was affected by scale effects for $We_1 <$ 1E+3 where We_1 is the inflow Weber number.

Remarks

For the lowest Froude number ($Fr_1 = 7$), Models 1 & 2 data showed strong dissymmetry which might be attributed to a feedback mechanism between the probe support and developing vortices. For $r > 0$, the probe support interfered with both sides of the developing shear region, preventing the development of helicoidal vortical structures. In turn, air entrapment was affected.

CONCLUSION

Air entrainment at vertical circular plunging jets was investigated for a range of flow conditions (Table 1). The project was focused on scale effects affecting air entrainment and bubble dispersion. Three scale models were used with jet nozzle diameters of 6.8, 12.5 and 25 mm. Detailed air-water measurement were performed systematically based upon a Froude similitude.

The study of air entrainment inception conditions showed that the inception velocity V_e is comparable to previous studies. Air concentration and bubble count rate results highlighted the advective diffusion of entrained air.

In Model 2, the mean pseudo-chord sizes were between 5 and 7 mm where the pseudo-bubble chord length $ch_{ab} = V_1 * t_{ch}$ was found to overestimate real bubble chords by 10 to 30%. Distributions of pseudo-bubble chord sizes ranged from less than 0.5 mm to more than 10 mm. The distributions were skewed with a preponderance of small bubbles. Significant scale effects when $We_1 < 1E+3$ or $V_1/u_r < 10$ in terms of void fraction and bubble count rate. For $We_1 < 1E+3$, the air entrainment rate is underestimated. For V_1/u_r less than ten, the detrainment rate is overestimated.

Overall the study demonstrates scale effects in small-size laboratory models of plunging jets. Further studies of the developing flow region should investigate air-water velocity distributions and turbulent velocity fluctuations.

ACKNOWLEDGMENTS

The authors acknowledge the financial support of the Australian Academy of Science, Japan Society for the Promotion of Science and Ministry of Education, Japan. H. CHANSON and S. AOKI thank their students for help and assistance : T. McGIBBON and B. BOLDEN (Australia), IWATA and KIDA (Japan).

REFERENCES

BIN, A.K. (1993). "Gas Entrainment by Plunging Liquid Jets." *Chem. Eng. Science*, Vol. 48, No. 21, pp. 3585-3630.

BRATTBERG, T., and CHANSON, H. (1998). "Air Entrapment and Air Bubble Dispersion at Two-Dimensional Plunging Water Jets." *Chemical Engineering Science*, Vol. 53, No. 24, Dec., pp. 4113-4127. Errata : Vol. 54, No. 12, p. 1925.

BRENNEN, C. (1970). "Cavity Surface Wave Patterns and General Appearance." *Jl of Fluid Mech.*, Vol. 44, Part I, p. 33.

CHANSON, H. (1997). "Air Bubble Entrainment in Free-Surface Turbulent Shear Flows." *Academic Press*, London, UK.

CHANSON, H. (1999). "The Hydraulics of Open Channel Flows : An Introduction." *Butterworth-Heinemann*, Oxford UK.

CHANSON, H., and BRATTBERG, T. (1998). "Air Entrainment by Two-Dimensional Plunging Jets: the Impingement Region and the Very-Near Flow Field." *Proc. 1998 ASME Fluids Eng. Conf.*, FEDSM'98, Washington DC, USA, June 21-25, Paper FEDSM98-4806, 8 pages (CD-ROM).

CHANSON, H., AOKI, S., and HOQUE, A. (2002). "Similitude of Air Bubble Entrainment and Dispersion in Vertical Circular Plunging Jet Flows. An Experimental Study with Freshwater, Salty Freshwater & Seawater." *Coastal/Ocean Engineering Report*, No. COE00-1, Dept. of Architecture and Civil Eng., Toyohashi University of Technology, Japan.

COMOLET, R. (1979). "Sur le Mouvement d'une bulle de gaz dans un liquide." *Jl La Houille Blanche*, No. 1, pp. 31-42.

CUMMINGS, P.D., and CHANSON, H. (1997a). "Air Entrainment in the Developing Flow Region of Plunging Jets. Part 1 Theoretical Development." *Jl of Fluids Eng.*, Trans. ASME, Vol. 119, No. 3, pp. 597-602.

CUMMINGS, P.D., and CHANSON, H. (1997b). "Air Entrainment in the Developing Flow Region of Plunging Jets. Part 2 : Experimental." *Jl of Fluids Eng.*, Trans. ASME, Vol. 119, No. 3, pp. 603-608.

CUMMINGS, P.D., and CHANSON, H. (1999). "An Experimental Study of Individual Air Bubble Entrainment at a Planar Plunging Jet." *Chem. Eng. Research and Design*, Trans. IChemE, Part A, Vol. 77, No. A2, pp. 159-164.

ERVINE, D.A., McKEOGH, E.J., and, ELSAWY, E.M. (1980). "Effect of Turbulence Intensity on the rate of Air Entrainment by Plunging Water Jets." *Proc. Instn Civ. Engrs*, Part 2, June, pp. 425-445.

GRIFFIN, O.M. (1984). "The Breaking of Ocean Surface Waves." *Naval Research Lab. Memo.*, Report No. 5337, Washington, USA.

HENDERSON, F.M. (1966). "Open Channel Flow." *MacMillan Company*, New York, USA.

HOYT, J.W., and TAYLOR, J.J. (1977). "Waves on Water Jets." *Jl of Fluid Mech.*, Vol. 83, Pt 1, pp. 119-127.

KOBUS, H. (1984). "Proceedings of International Symposium on Scale Effects in Modelling Hydraulic Structures." IAHR, Esslingen, Germany, H. KOBUS Editor.

KOLANI, A.R., OGUZ, H.N., and PROSPERETTI, A. (1998). "A New Aeration Device." *Proc. 1998 ASME Fluids Eng. Summer Meeting*, 21-25 June 1998, Washington, D.C., USA 257, 111-145.

WOOD, I.R. (1991). "Air Entrainment in Free-Surface Flows." *IAHR Hydraulic Structures Design Manual No. 4*, Hydraulic Design Considerations, Balkema Publ., Rotterdam, The Netherlands, 149 pages.

ZHU, Y.G., OGUZ, H.N., and PROPERETTI, A. (2000). "On the mechanism of air entrainment by liquid jets at a free surface." *Jl Fluid Mech.*, Vol. 404, pp. 151-177.